7528–7540 *Nucleic Acids Research, 2012, Vol. 40, No. 15* *Published online 21 May 2012*
doi:10.1093/nar/gks356

A small ribozyme with dual-site kinase activity

Elisa Biondi[1,2,*], Adam W.R. Maxwell[1,2] and Donald H. Burke[1,2,*]

[1]Department of Molecular Microbiology and Immunology and [2]Department of Biochemistry, Bond Life Sciences Center, University of Missouri School of Medicine, Columbia, MO 65211, USA

Received November 22, 2011; Revised April 8, 2012; Accepted April 10, 2012

ABSTRACT

Phosphoryl transfer onto backbone hydroxyls is a recognized catalytic activity of nucleic acids. We find that kinase ribozyme K28 possesses an unusually complex active site that promotes (thio)phosphorylation of two residues widely separated in primary sequence. After allowing the ribozyme to radiolabel itself by phosphoryl transfer from [γ-^{32}P]GTP, DNAzyme-mediated cleavage yielded two radiolabeled cleavage fragments, indicating phosphorylation sites within each of the two cleavage fragments. These sites were mapped by alkaline digestion and primer extension pausing. Enzymatic digestion and mutational analysis identified nucleotides important for activity and established the active structure as being a constrained pseudoknot with unusual connectivity that may juxtapose the two reactive sites. Nuclease sensitivities for nucleotides near the pseudoknot core were altered in the presence of GTPγS, indicating donor-induced folding. The 5′ target site was more strongly favored in full-length ribozyme K28 (128 nt) than in truncated RNAs (58 nt). Electrophoretic mobilities of self-thiophosphorylated products on organomercurial gels are distinct from the 5′ mono-thiophosphorylated product produced by reaction with polynucleotide kinase, potentially indicating simultaneous labeling of both sites within individual RNA strands. Our evidence supports a single, compact structure with local dynamics, rather than global rearrangement, as being responsible for dual-site phosphorylation.

INTRODUCTION

The RNA world hypothesis posits that early biological catalysts were RNA or RNA-like molecules. A prediction of this scenario is that nucleic acid sequences should exist that catalyze most of the chemical reactions needed to sustain a minimal viable cell. Indeed, *in vitro* selections have identified artificial ribozymes that catalyze oxidoreduction (1,2), several mechanisms of carbon-carbon bond formation (3–9) and the group transfer reactions that underlie protein (3–8) and polynucleotide synthesis (9–11), in addition to assembly of RNA-nickel-amino acid (12) nanostructures and several other reactions [reviewed in (13,14)]. Uncovering the functional versatility and catalytic proficiency of ribozymes helps to constrain RNA world theories and generates tools that could potentially be used to re-engineer cellular metabolisms, while also adding to our understanding of macromolecular catalysis.

Nucleic acid-catalyzed phosphoryl transfer is especially of interest because of the ubiquitous importance of phosphorylation in biology. Work from our laboratory and others has established that sequence space is populated with a large number of structured RNA and DNA molecules that catalyze self-phosphorylation or self-thiophosphorylation of internal or terminal backbone hydroxyls (15–23). Several of these have been analyzed for their structural, dynamic and mechanistic features. For example, ribozyme 2PT3.1 catalyzes multiple-turnover hydrolysis of ATPγS by a phosphoenzyme intermediate (16,17). Early kinetic studies of ribozyme Kin.46 provided the first mechanistic insights into kinase ribozyme function (15,20). Later analysis of the effects of specific Kin.46 mutations on kinase activity and the temperature dependence of the reaction rate identified specific nucleotides required for catalysis and activation (24) and provided interhelical distance constraints (25). Most kinase ribozymes and DNAzymes are highly specific in their ability to use only the Nucleotide triphosphate (NTP) donor for which they were selected, although at least one DNAzyme uses NTPs promiscuously (21). Donor recognition can extend beyond the nucleobase, with consequences for phosphoryl transfer mechanism. A recent analysis of competitive inhibition by donor analogs provided the first demonstration that many kinase ribozymes interact with one or more of the donor phosphates, potentially facilitating catalysis

*To whom correspondence should be addressed. Tel: +1 573 884 5159; Fax: +1 573 884 9395; Email: biondie@missouri.edu
Correspondence may also be addressed to Donald H. Burke. Fax: +1 352 271 7076; Email: burkedh@missouri.edu
Present address:
Dr Biondi, Foundation for Applied Molecular Evolution (Ffame), 720 SW Second Avenue, Suite 201, Gainesville, FL 32601, USA.

by orienting and reducing the entropy of the gamma (thio)phosphate (18).

Kinase ribozymes described to date have all been selected by incubating RNA libraries with ATPγS and/or GTPγS and then taking advantage of the unique chemical properties of sulfur to recover RNA species that acquired a thiophosphoryl group. Kinase ribozymes selected for thiophosphoryl transfer are generally also able to promote phosphoryl transfer, albeit at significantly reduced rates. However, selection strategies based on sulfur acquisition place no constraints on the number or location of thiophosphorylation sites among the recovered RNAs. For example, Kin.46 phosphorylates a terminal 5′OH, but many other RNAs phosphorylate internal 2′OH sites that can usually be mapped by partial alkaline digestion of 5′-radiolabeled, self-thiophosphorylated molecules. When the digested products are separated on denaturing sequencing gels, the modified sites appear clearly as single gaps in the digestion pattern (16,20). Applying this analysis to a collection of eight recently described kinase ribozymes yielded unambiguous and unique phosphorylation sites within seven of the eight ribozymes analyzed, revealing a strong preference for (thio)phosphorylation at the 2′OH of internal guanosine residues in those RNAs (18).

Ribozyme K28 presented an unusual exception. Although this RNA was proficient in generating thiophosphorylated product, it was not possible to use a similarly straightforward approach to map its phosphorylation site. We recently undertook a detailed examination of the perplexing mechanistic and structural questions posed by this ribozyme, part of which is described elsewhere (E. Biondi *et al*., submitted for publication). In the present work, we establish that ribozyme K28 self-(thio)phosphorylates on two different nucleotides in the presence of GTP(γS), despite there not having been any specific selection pressure for such dual-site catalytic activity. Ribozymes with dual-site kinase activity have not previously been characterized. Therefore, we performed mutational analysis, enzymatic digestions and comparative sequence analysis to define which nucleotides are important for activity. We find that the active structure comprises a pseudoknot that appears to juxtapose the two reactive nucleotides. Interestingly, auto-phosphorylation at both sites was observed for numerous truncated mutants, and at least one version of the ribozyme [K28(1–77)C] generates an electromorph on organimercurial gels that is distinct from 5′-mono-thiophosphorylated RNA, raising the possibility that both sites acquire thiophosphate at the same time within a given RNA strand. These results are discussed in terms of potential mechanisms for the dual-site kinase reaction.

MATERIALS AND METHODS

Materials

Oligodeoxynucleotides were purchased from Integrated DNA Technologies (IDT, Coralville, IA, USA). RNA was transcribed *in vitro* using phage T7 RNA polymerase, which was overproduced in bacteria and purified in the laboratory. Other enzymes were purchased from New England Biolabs (Ipswitch, MA, USA), Ambion (Austin, TX, USA) and Amersham Biotech (Pittsburgh, PA, USA), and these enzymes were used with the corresponding commercial buffers. ATPγS and GTPγS were purchased from Sigma (St Louis, MO, USA). Radiolabeled nucleotides for labeling 5′OH, internal phosphates or internal 2′OH positions ([γ^{32}P]-ATP, [α^{32}P]-CTP and [γ^{32}P]-GTP, respectively) were purchased from Perkin-Elmer (Waltham, MA, USA). *N*-acryloyl-aminophenylmercuric chloride (APM) was prepared as described (26,27).

Self-kinase reactions

Internally radiolabeled transcripts were gel purified, unfolded in water at 85°C for 5 min, then refolded on ice for 5 min by addition of 5× self-phosphorylation (SP) buffer (1× SP buffer = 6 mM $MgCl_2$, 0.2 mM $CaCl_2$, 0.5 mM $MnCl_2$, 0.01 mM $CuCl_2$, 200 mM KCl, 15 mM NaCl, 25 mM hydroxyethylpiperidine ethanesulfonate (HEPES), pH 7.4). Kinase reactions utilized 1 μM RNA [50 000–200 000 cpm] and were initiated by adding GTPγS to a final concentration of 1 mM and moving the reaction mixtures to 32°C. Reactions were quenched at various times in stop buffer [95% formamide, 15 mM ethylenediaminetetraacetic acid (EDTA), containing trace amounts of xylene cyanol and bromophenol blue as tracking dyes]. Products were separated on 8% denaturing trilayered APM gels (27,28). Autoradiographs were obtained with a FLA-5000 phosphorimager (FujiFilm) and analyzed with MultiGauge software. The fraction of the RNA converted to product at a given time was calculated by dividing the intensities of RNA retained at the APM interface by the total of all the bands within each lane. These fractions are reported directly without background subtraction (typical background 0.5–2.0% of total).

Phosphorylation site mapping and calculation of site preference ratios by DNAzyme-mediated RNA cleavage analysis

Ribozymes K28, K28(1–98) and K28(1–77) were transcribed *in vitro* without radiolabel, then gel purified and refolded as described earlier. RNA-catalyzed SP reactions were performed in 20 μl by incubating 1 μM RNA with 1.7 μM [γ-^{32}P]GTP as phosphoryl donor to radiolabel the RNAs at the sites of SP. Reactions were moved to ice after 16 h, ethanol precipitated twice to remove excess GTP and resuspended in water. After aliquotting into DNAzyme solutions (in 50 mM Tris–Cl, pH 8.0), the mixtures were denatured at 95°C and slowly cooled to 4°C at 0.1°C/s to anneal the DNAzyme to the RNA. Digestions were initiated by adding $MgCl_2$. Final concentrations of all components in these reactions were 1 μM RNA, 1.5 μM DNAzyme, 15 mM $MgCl_2$, 50 mM Tris–Cl, pH 8.0. After 1 h at 37°C, reactions were stopped by ethanol precipitation. Pellets were resuspended in gel-loading buffer, heated for 5 min at 95°C, cooled on ice and analyzed by 10–18%, 8 M urea denaturing polyacrylamide gel electrophoresis (PAGE). Autoradiographs were obtained as described earlier. Sequences of the

DNAzymes used in this study are reported in Supplementary Table S1. For calculating site preference ratios, RNAs were allowed to self-radiolabel as mentioned earlier and were then digested with DNAzyme Dzy5. Digested products were separated on a denaturing gel and quantified by phosphorimaging. Site preference ratios (R) were calculated as $R = P_{5'}/P_{3'}$, where $P_{5'}$ is the signal for the band corresponding to phosphorylation at the 5′ site, and $P_{3'}$ is the signal for the band corresponding to phosphorylation at the 3′ site.

Phosphorylation site mapping by alkaline digestion

Ribozyme K28 was labeled with ^{32}P on its 5′ terminus using [γ-^{32}P]ATP and polynucleotide kinase (PNK), gel purified, subjected to overnight self-thiophosphorylation and purified on an 8% trilayer APM gel as mentioned earlier. Alkaline digestions of Dithiothreitol (DTT)-extracted products were performed in 100 mM Na_2CO_3, pH 9.0, 2 mM EDTA for 15 min at 90°C. Alkaline digestions of control RNAs were performed in 50 mM Na_2CO_3, pH 9.0, 1 mM EDTA for 10 min at 90°C. Ribonuclease T1 digestions under denaturing conditions (0.1 U/μl T1 in 0.025 M Na-citrate, 7 M urea, 10.5 mM EDTA, pH 8.0, at 55°C for 10 min) served as size standards.

Thiophosphorylation site mapping by reverse transcription pausing

Self-thiophosphorylated RNAs were purified from denaturing trilayer APM gels as mentioned earlier, and the purified products were used as templates in reverse transcription (RT) reactions. RNAs were mixed with 5′-^{32}P-labeled primers, heated to 95°C for 5 min and slow cooled to 4°C (0.1°C/s) to anneal primer with template. RT reactions were initiated by the addition of 5 U/μl moloney murine leukemia virus (M-MLV) reverse transcriptase (Promega) and performed at 37°C in 50 mM Tris–HCl, pH 8.3, 75 mM KCl, 3 mM $MgCl_2$ and 10 mM DTT. Time points here taken immediately after addition of enzyme (0 min) and at 2, 5 and 10 min. Aliquots were quenched in stop buffer and analyzed on 12% denaturing sequencing gels.

Secondary structural analysis by enzymatic probing

The 5′ radiolabeled RNA (50 000–200 000 cpm) was digested under native conditions at 32°C with ribonuclease T1 (Ambion, 0.005 U/μl for 2 min), S1 nuclease (New England Biolabs, 4.75 U/μl for 10 min) or ribonuclease V1 (Ambion, 5×10^{-5} U/μl for 8 min). Size ladders were generated by alkaline ribonuclease T1 digestion of control RNAs as described earlier. All reactions were quenched with equal volumes of colorless gel loading buffer (10 M urea, 15 mM EDTA) and quickly cooled in a dry ice/ethanol bath. Products of digestions were separated on 8 M urea denaturing 15% polyacrylamide gels and analyzed by phosphorimaging. Initial secondary structures were calculated with the online web servers of the programs mFold (29) and MC-fold (30).

Comparing PNK reaction with ATPγS and self-labeling reactions with GTPγS using gels with uniform APM

To prepare samples and controls for evaluating different forms of thiophosphorylated RNA, 244 pmoles of internally ^{32}P-labeled ribozyme K28(1–77)C RNA ('sample 1') was dephosphorylated with Calf Intestinal Phosphatase (1.22 μM RNA, 30 U Calf Intestinal Phosphatase (CIP), 1× commercial CIP buffer, 1 h at 37°C) extracted with phenol–chloroform (phenol–chloroform–isoamyl alcohol in 25:24:1 ratio), ethanol precipitated and resuspended in 30 μl H_2O to yield 'sample 1A' (6.5 μM). Samples 2–7 were then prepared from sample 1 A as detailed later, followed by organic extraction, two ethanol precipitations and resuspending the samples in 10 μl H_2O plus 50 μl gel loading buffer (Figure 6A).

Sample 2 was simply a 5-μl aliquot of sample 1 A. Samples 3 and 4 were generated by treating separate 5 μl aliquots of sample 1 A with PNK in the presence of either ATP (Sample 3) or ATPγS (Sample 4) (2.6 μM RNA, 10 U PNK, 1× PNK-buffer, 1 mM ATP or ATPγS, 45 min at 37°C). For Samples 5–7, 15 μl of Sample 1 A was allowed to self-thiophosphorylate (1 μM RNA, 1× SP buffer, 1 mM GTPγS, 18 h at 32°C), ethanol precipitated twice and resuspended in 15 μl H_2O; 5 μl of this material constituted Sample 5. Separate 5 μl aliquots of the self-thiophosphorylated RNA were treated with PNK as mentioned earlier in the presence of ATPγS (Sample 6) or ATP (Sample 7). One-third of each sample in gel-loading buffer was loaded onto 8% denaturing (8 M urea) gel that also contained 0.1 μg/ml APM. Autoradiograms were obtained and analyzed as described earlier.

RESULTS

A dual-site acting kinase ribozyme

To gain better insight into the location(s) of the phosphorylation site(s) in ribozyme K28, non-radiolabeled RNA was allowed to self-phosphorylate in the presence of γ-[^{32}P]-GTP as phosphoryl donor, so that any site that would normally acquire a thiophosphoryl group from GTPγS will instead be tagged with radiolabel. The modified RNA was then digested with engineered variants of DNAzymes '8-17' (cleaves GˆA) and '10-23' (cleaves YˆR) (31) (Figure 1). DNAzyme Dzy1 cleaves after Position 8, producing two fragments of sizes 8 and 118 nt. Similarly, DNAzyme Dzy2 cleaves after Position 16. Both these DNAzymes yielded two radiolabeled digestion products (Figure 1B). Since the only radioactive signal comes from RNA-catalyzed phosphotransfer, the presence of two labeled RNA fragments clearly indicates that K28 self-phosphorylates in more than one position. Ribozyme K28 and its truncated version K28(1–77)—for which the 5′ and 3′ termini are at positions 1 and 77 of parent ribozyme K28—were then analyzed by digestion with DNAzymes Dzy3 (cleaves after position 27), Dzy4 (Position 38) and Dzy5 (Position 59). As was observed for Dzy1 and Dzy2, DNAzyme digestion yielded two new radioactive fragments for Dzy3, Dzy4 and Dzy5 (Figure 1C), whereas for Dzy6 (Position 75) only a

single digested fragment retained the radiolabel (data not shown). These data clearly establish that these ribozymes self-phosphorylate at two distinct sites. They further constrain the 5′ phosphorylation site to be within the nucleotide regions 1–7 (upstream of the cleavage site for Dzy1) and the internal site in the nucleotide regions 60–74 (between the cleavage sites for Dzy5 and Dzy6).

Mapping the two sites of (thio)phosphorylation

Two methods were used to map the sites of phosphorylation with greater resolution. First, self-thiophosphorylated ribozyme K28 was purified from a trilayer APM gel and subjected to alkaline digestion, then separated on a high-resolution gel alongside control RNAs and non-thiophosphorylated RNA that had been similarly digested (Figure 2A). The digested fragments of self-thiophosphorylated RNA showed two overlapping patterns. In the major pattern, the bands are shifted upwards in Lanes 1 and 2 relative to Lanes 3 and 4, as we have observed previously for fragments that carry a thiophosphoryl modification (18). This shift is readily apparent on comparing T1 digestion patterns in Lanes 1 and 4 and is further confirmed by sequence-specific variations in band intensities in Lanes 2 and 3 (e.g., see A15 and C17, which are especially dark). Interestingly, the intensities of the bands in the major, shifted patterns are roughly equal at every position near the 5′-end all the way down to G2, indicating that the thiophosphorylation site is upstream of nucleotide G2. This analysis identifies nucleotide G1 as the acceptor substrate for thiophosphorylation. Since the 5′OH of this residue was not available during the original selection (18), the site of thiophosphorylation is most likely the 2′OH. Overlapping with this major pattern, there is also a minor pattern of fainter bands (small text labels) that align exactly with the alkaline ladder from the non-thiophosphorylated, alkaline-digested RNA (Lane 3).

Overlapping signals from the two patterns in the alkaline digestion analysis obscured the internal thiophosphorylation site within the nucleotide regions 59–75 (Figure 2A). Therefore, 5′-radiolabeled primers were used to generate complementary DNA (cDNA) from ribozyme K28 before and after incubation with GTPγS. Truncated variant K28(1–98) was similarly analyzed for comparison. M-MLV RT is known to pause near sites of internal 2′ thiophosphorylation (32,33). Ribozymes K28 and K28(1–98) gave equivalent pausing patterns (Figure 2B and C, respectively, and data not shown). A ladder of partially extended cDNA products within several of the lanes allowed facile band assignments, some of which is annotated explicitly in Figure 2. For both ribozymes, thiophosphorylation-dependent pauses are evident at A3 and U67. The pause at A3 is attributed to 2′ thiophosphorylation of G1, indicating that cDNA

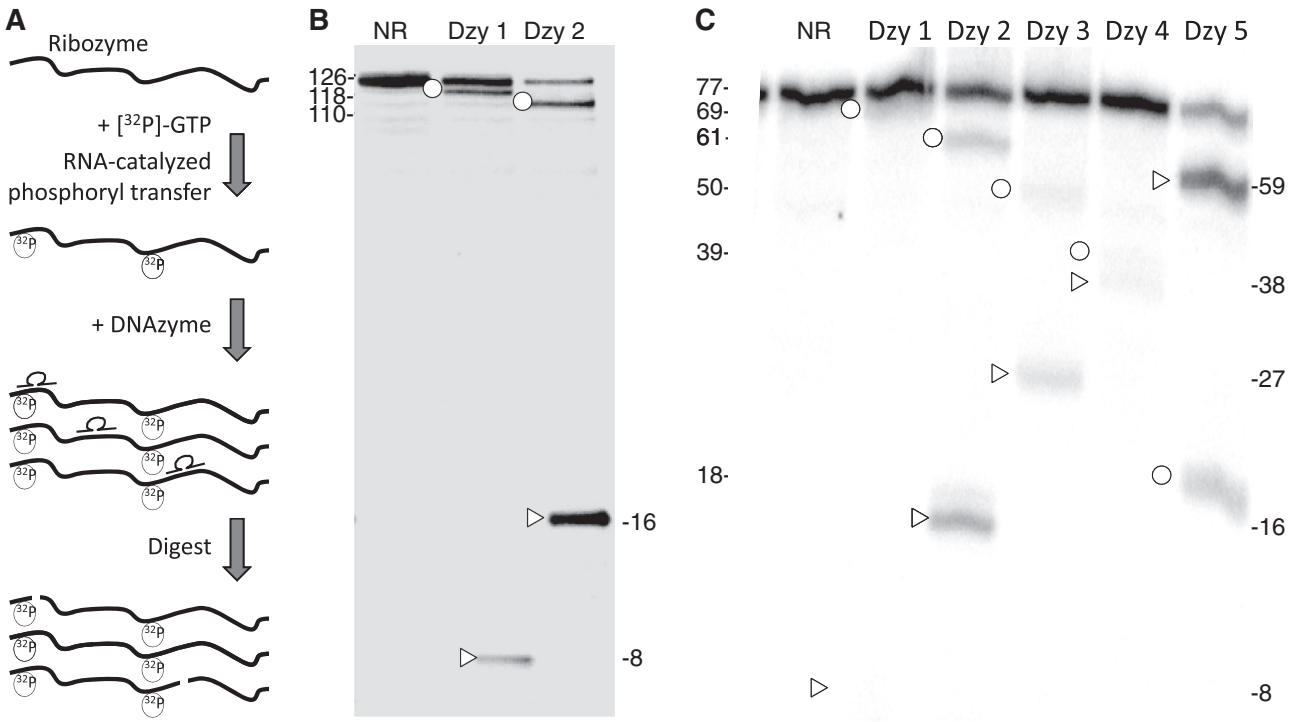

Figure 1. Dual-site phosphorylation by ribozyme K28. (**A**) Schematic of DNAzyme assay. In brief, ribozymes were allowed to self-phosphorylate with [γ-^{32}P]GTP, then digested with DNAzymes targeted to cleave specific sites within the RNA, followed by denaturing PAGE analysis. Additional details are given in the text. The sizes of the fragments that acquire radioactivity delimit the locations of the two phosphorylation sites. (**B**) Representative data for ribozyme K28 (126 nt; 18% polyacrylamide). (**C**) Representative data for ribozyme K28(1–77) (77 nt, 12% polyacrylamide). DNAzymes used in each assay are indicated above the lanes. Dzy6 was omitted from analysis of K28(1–77) because its cleavage site after position 65 is only two nucleotides from the 3′-end of the RNA. 'NR', no DNAzyme treatment; open circles, fragments in which the RNA has radiolabeled itself on the 5′ side of the cleavage site (fragment sizes indicated on the left); open triangles, radiolabeled fragments on the 3′ side of the cleavage site (fragment sizes are indicated on the right). The most complete DNAzyme digestions were obtained with Dzy5.

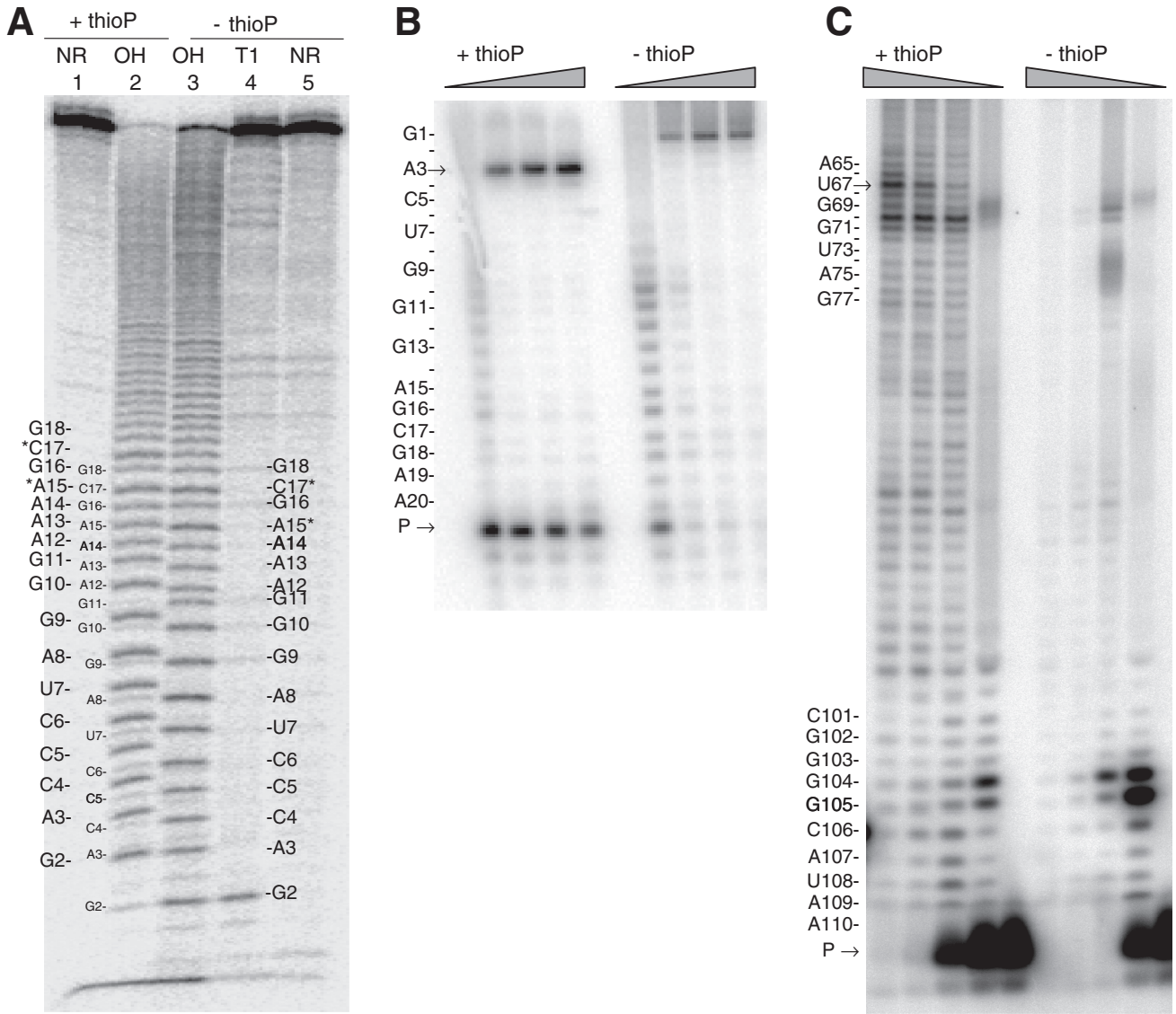

Figure 2. Identifying the sites of self-thiophosphorylation. (**A**) Ribozyme K28 was thiophosphorylated with GTPγS and purified on organomercurial gel ('+ thioP' lanes), then subjected to partial alkaline digestion (OH) or was digested directly without prior thiophosphorylation ('– thioP' lanes). NR and T1 indicate RNAs that were not digested or that were digested with ribonuclease T1, respectively. Major bands are labeled in larger font and the minor secondary pattern with smaller font, as detailed in text. Asterisks on A15 and C17 illustrate examples of the use of position-specific variation in band intensity to assign nucleotide identities within the '+ thioP' lane. (**B**) Radiolabeled cDNA primers were annealed to ribozyme K28 at an internal position. RT reactions were quenched at increasing times (wedge above gels): a few seconds and at 2, 5 and 10 min after adding the RT enzyme. Partial extension products are marked with nucleotide identities. P indicates the unextended primer. (**C**) Same as panel (B) but using a primer that anneals at the 3′-end of the RNA. Note thiophosphorylation-independent pauses at runs of G's near the bottom of the gel (G104 and G105) and just before reaching the downstream thiophosphorylation site (G70), reflecting RT's propensity to pause at homopurine tracts (33).

synthesis stops two nucleotides before the modification in this context. Applying this same metric to the pause at U67 places the internal self-thiophosphorylation site at A65. An alternative metric based on pausing immediately adjacent to sites of 2′OH thiophosphorylation (32) would place the internal site at nucleotide C66. Thus, current data are consistent with either A65 or C66 as being the internal modification site.

Delimiting the functional boundaries

To define the 5′ and 3′ sequence boundaries of the functional core, end point self-thiophosphorylation yields in overnight reactions were measured for a series of truncation variants of ribozyme K28 (Table 1 and Supplementary Figure S1). The yield of thiophosphorylated product was not significantly affected by removing up to 48 nt from the 3′-end [ribozymes K28(1–98), K28(1–93), K28(1–88), K28(1–83), K28(1–78)], but yield was barely above background for deletions of 53 or more nucleotides from the 3′-end [ribozymes K28(1–73), K28(1–68), K28(1–63), K28(1–58), K28(1–53)] (Table 1). To map more precisely the 3′-end of the functional core, additional truncations were generated that removed one nucleotide at a time between positions 73 and 78. Self-thiophosphorylation

Table 1. Dual-sites reactivity for shortened ribozymes

Ribozyme	Size, nt	Nucleotides present	Relative self-thiophosphorylation yield[a]	Dual-site reactivity	Relative site preference	Site preference ratio[b]
K28	126	1–126	58	Yes	73:27	2.70
K28(1–98)[c]	98	1–98	100	Yes	77:23	3.35
K28(1–98)A74U[c]	98	1–98	63	Yes		
K28(1–98)A75U[c]	98	1–98	13	ND		
K28(1–98)U76A[c]	98	1–98	21	Yes		
K28(1–98)G77C[c]	98	1–98	43	Yes		
K28(1–98)U78A[c]	98	1–98	72	Yes		
K28(1–98)G79C[c]	98	1–98	100	Yes		
K28(1–98)_InvStem2a[c]	98	1–98	94	Yes		
K28(11–98)	88	11–98	1[d]	ND		
K28(16–98)	83	16–98	1[d]	ND		
K28(1–93)	93	1–93	78	Yes		
K28(1–88)	88	1–88	81	Yes		
K28(1–83)	83	1–83	85	Yes		
K28(1–78)[c]	78	1–78	86	Yes		
K28(1–77)[c]	77	1–77	103	Yes	71:29	2.45
K28(1–77)A[c]	66	1–19_UUCG_35–77	53	Yes	63:37	1.70
K28(1–77)B[c]	58	1–16_UUCG_40–77	106	Yes	59:41	1.44
K28(1–77)C[c]	58	1–12_UAGCUU CGGCUA_44–77	107	Yes	58:42	1.38
K28(1–76)[c]	76	1–76	43	Yes		
K28(1–75)[c]	75	1–75	37	Yes		
K28(1–74)[c]	74	1–74	19	ND		
K28(1–73)[c]	73	1–73	8	ND		
K28(1–68)	68	1–68	1[d]	ND		
K28(1–63)	63	1–63	1[d]	ND		
K28(1–58)	58	1–58	1[d]	ND		
K28(1–53)	53	1–53	4[d]	ND		

[a]Self-thiophosphorylation yield (percent conversion to product) is shown relative to the yield of ribozyme K28(1–98), which reached a self-labeling plateau of 51.3% ± 1.5%.
[b]Site preference ratios were determined as described in 'Materials and Methods' section. ND, not determined.
[c]Ribozymes for which structures and/or sequence details are shown in Figure 4.
[d]Indistinguishable from background under the conditions tested.

yield was unperturbed for ribozyme K28(1–77), which terminates at G77, but rapidly decreased with each subsequent nucleotide removed. The last nucleotide required for achieving maximal yield is therefore G77. Removing 10 or 15 nt from the 5′-end [ribozymes K28(11–98) and K28(16–98), respectively] eliminated all kinase activity, not only at the now-missing 5′ site within the deleted region but also at the 3′ site, probably due to the involvement of this region in forming the functional secondary structure, as detailed later.

Enzymatic probing of secondary structure and donor binding site

To define the key helical elements, ribozymes K28 and K28(1–98) were subjected to enzymatic digestion. 5′-radiolabeled RNAs were refolded and digested in reaction buffer with the enzymes RNase T1 (cuts after each single-stranded G), nuclease S1 (cuts ssRNA) and RNase V1 (cuts dsRNA). The digestion patterns for the two molecules were very similar (Supplementary Figure S2) and were used as constraints to generate an initial secondary structure (Figure 3A). A 19-nt internal loop on the 3′ strand divides the long base-paired stem of this model into a discontinuous upper segment (paired regions P2a and P2b) and a continuous lower segment (P1) that is flanked by single-stranded segments on each end.

When similar enzymatic digestions were performed in the presence or absence of 1 mM GTPγS, cleavages at nucleotides U54, A59, U60 and G61—all of which are located within the large internal loop—were clearly modulated by the presence of the donor (Figure 3B). Enzymatic digestions are insensitive to donor in the regions 77–95 (for T1), 34–46 (for V1) and 24–30 (for S1), among others, allowing these regions to serve as controls. These results suggest structural rearrangements on interaction with the donor that lead to an increase in overall paired structure at nucleotides A59, U60 and G61 (increased V1 cleavage and decreased S1 cleavage) and decreased structure at U54 (reduced V1 cleavage).

Mutational analysis defines the functional secondary structure

The nucleotide sequence requirements and core functional secondary structure of ribozyme K28 were defined through a comprehensive mutational analysis (Figure 4A and Table 1). To test the significance of stem P1, nucleotides on the 5′ side of the stem were replaced with their Watson–Crick counterparts to disrupt base pairing within the context of ribozyme K28(1–77). These modifications severely compromised self-thiophosphorylation (5- to 10-fold reduction) for both stem-disrupted variants, but product yield was fully restored and even improved on

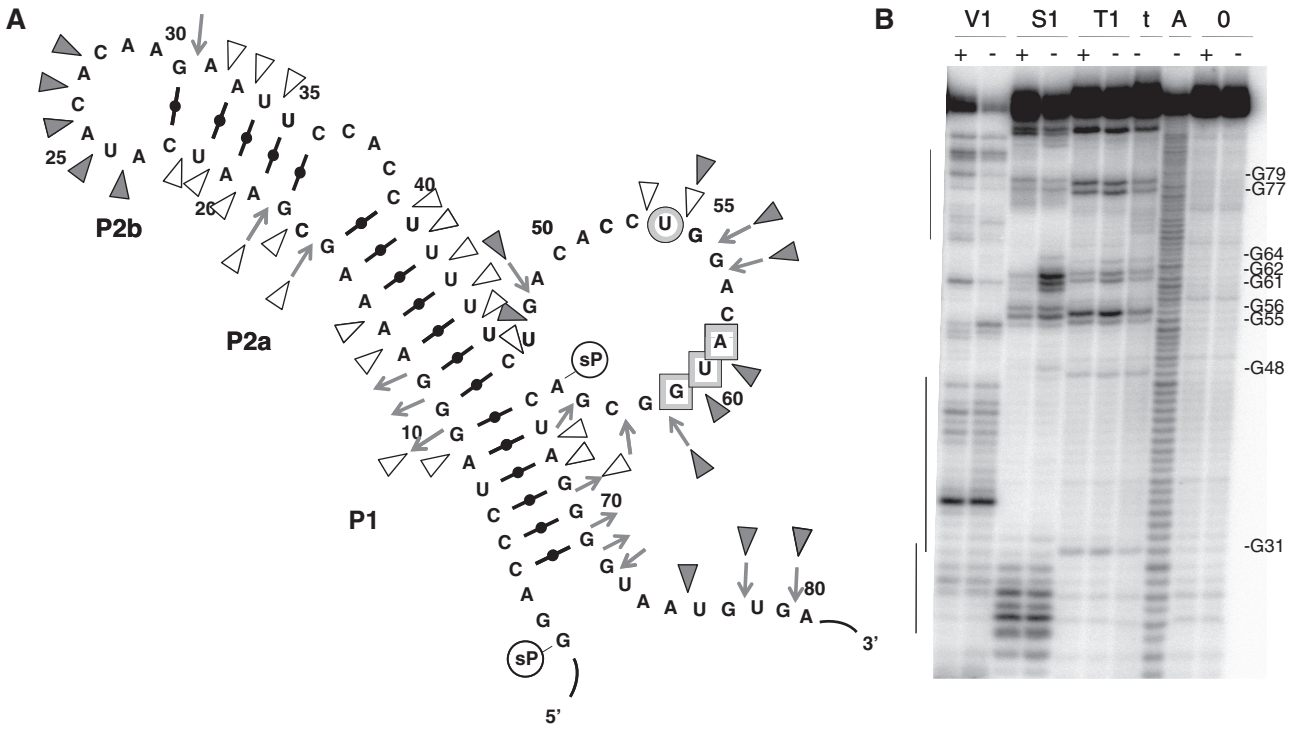

Figure 3. Enzymatic probing reveals initial secondary structure and nucleotides subject to donor-induced folding. (**A**) Summary of enzymatic probing data for ribozymes K28 and K28(1–98) in SP buffer (see Supplementary Figure S2 for representative raw gel data). Digestion data are mapped onto secondary structure model of K28(1–98), omitting the 3′ terminal 18 nt. Filled triangles, S1 nuclease (cleaves unstructured RNA); open triangles, V1 nuclease (cleaves double-stranded RNA): inward-pointing arrows, ribonuclease T1 (cleaves after unstructured G residues); outward-pointing arrows, G residues that are not cleaved by ribonuclease T1 under native conditions. Sites of phosphorylation (as determined in Figure 2) are indicated with 'sP'; nucleotides within shaded squares or circles change their reactivity to enzymatic digestion in a manner indicating increased (or decreased, respectively) structure on interaction with the donor. Nucleotides 1–32 (shown) and 103–126 (not shown) were held constant during the original selection. (**B**) Enzymatic digestion of K28(1–98) in the presence (+) or absence (−) of the thiophosphoryl donor GTPγS by nucleases V1, S1 and T1 as indicated above the gel. Lower case 't', nuclease T1 digestion under denaturing conditions; 'A', alkaline digestion; '0', non-digested RNA. GTPγS modulates RNA sensitivity in the region U54 to G64 but not in the regions 77–95 (for T1), 34–46 (for V1) and 24–30 (for S1) indicated by vertical lines and noted in the text. Note that nucleases S1 and V1 yields 3′OH termini, in contrast to the other cleavage mechanisms, which leave 2′,3′-cyclic phosphate termini (34,35); the S1 and V1 patterns are therefore shifted upward by about 1 nt relative to the others.

introducing additional mutations into the 3′ side of the stem to rescue base pairing (Figure 4A, bottom left). Thus, P1 is confirmed as being an important element in the K28 core.

The contribution of P2 was similarly evaluated. Within the context of ribozyme K28(1–98), changing the first 6 nt (GGAAAA) on the 5′ side of P2a to a polypyrimidine tract (CUUUUU) greatly reduced thiophosphorylation, whereas normal yield was rescued by introducing compensatory mutations in the 3′ side of the stem (Figure 4A, top). The more peripheral P2b was successively removed from the smaller ribozyme K28(1–77) by replacing 15 or all 23 nt with a UUCG tetraloop to generate ribozymes K28(1–77)A and K28(1–77)B. The 5′ and 3′ termini of these ribozymes are at positions 1 and 77 of parent ribozyme K28, and the suffixes A and B denote their respective internal deletions. Product yields for both ribozymes were equivalent to that of ribozymes with intact P2b, indicating that P2b is dispensible. Within this P2b-deleted context, strengthening P2a by changing three of the last four base pairs to generate ribozyme K28(1–77)C had no deleterious effect. These results support the presence of P2a as being an important element in the K28 core.

The deletion analysis mentioned earlier for delimiting the functional boundaries established that at least 6 nt are required downstream from P1. To investigate whether the identities of these nucleotides are important for self-thiophosphorylation by this ribozyme, Watson–Crick transversion mutations were introduced at positions 74–79 of ribozyme K28(1–98). Single mutations A74U, U78A and G79C were all well tolerated (less than 2-fold reduction in product yield), whereas single mutations A75U, U76A and G77C all compromised thiophosphorylation by >2-fold. Sensitivity to mutations at these positions is consistent with the observation mentioned earlier that G77 is the last required nucleotide (Figure 4A, bottom right). Pairing of the nucleotides at Positions 75–77 with potential partners within the large loop to form Stem P3 would generate a pseudoknotted structure. To test the contributions of this putative P3, disruptive and compensating mutations were introduced into this element in the context of ribozyme K28(1–77), taking care to minimize alterations to the nucleotides that

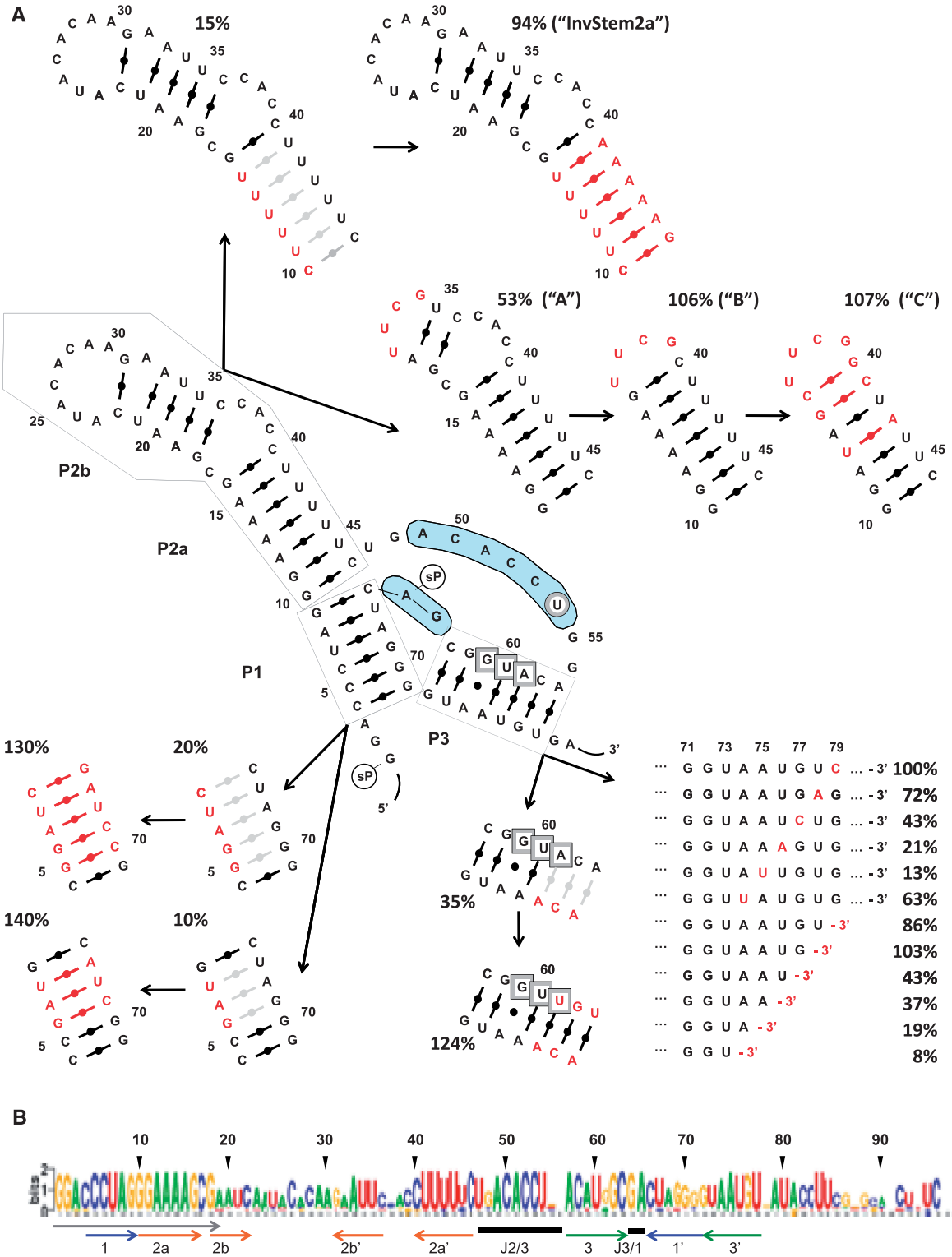

Figure 4. Mutational analysis of truncated K28 variants. (**A**) The indicated mutations were introduced into either K28(1–98) or K28(1–77). Self-thiophosphorylation yields for each mutant are indicated next to the corresponding mutation, in each case taking the unmutated reference sequence [K28(1–77) or K28(1–98)] as 100%. Altered nucleotides and rescued pairing interactions are indicated in red; disrupted pairing interactions are in gray. Ribozymes K28(1–77)A ('A'), K28(1–77)B ('B'), K28(1–77)C ('C') and InvStem2a, which are discussed in the text or in Table 1, are indicated. Inset in bottom right indicates yields for ribozyme K28(1–98) mutated at specific sites between nucleotides 73 and 78 or terminating at the indicated nucleotides. Highlighted nucleotides in single-stranded joining regions J2/3 and J3/1 were perfectly conserved in mutation/reselection analysis (Supplementary Figure S3). (**B**) 'RNALogo' depiction of information content at each position, as generated from aligned sequences derived from the mutation/reselection, using the online server at http://rnalogo.mbc.nctu.edu.tw/ (36). Arrows beneath the alignment refer to the 5′ primer-binding constant region (gray), secondary structural elements (color coded) and joining regions (black lines below and gray box within alignment).

demonstrated nuclease sensitivity in the presence of GTPγS. The mutant with the weakened P3 produced about one-third as much product in the overnight reaction as did the unmutated reference sequence. In contrast, simultaneously introducing compensatory mutations in the 5′ side of P3 restored full product yield (Figure 4A, bottom right). These results confirm P3 as an important structural element in the K28 core and provide a rationalization for both the 3′ truncation and point mutation data. An additional and intriguing possibility is that binding of GTPγS may stabilize P3 to provide the underlying basis for donor-dependent alteration of nuclease sensitivities observed earlier.

Sequence constraints in single-stranded joining regions revealed by mutation/reselection

A DNA template for ribozyme K28(1–118) was synthesized with a mutational density of 15% per position in nucleotides 19–98. The corresponding RNA was then subjected to five cycles of reselection for self-thiophosphorylation under essentially the same conditions as those used during the selection that gave rise to the K28 parent (18). The information content of aligned sequences from 40 isolates derived from this reselection was analyzed using the online RNALogo software (36) (Figure 4B; Supplementary Figure S3). At this mutational density, approximately six mutations are expected to be observed at any given position among the 40 aligned sequences, and regions shown above to be dispensable (such as P2b) display mutation rates in this range. In contrast, the single-stranded regions, 5′-UgA**CACCU**gg-3′ within J2/3 and 5′-**GA**-3′ within J3/2, display perfect conservations (bold) or very strong conservation (underlined, only one or two mutations) at 9 of the 12 single-stranded positions (light blue highlight in Figure 4A). Residue A65 implicated as the internal thiophosphorylation site is among the perfectly conserved sites. These evolutionary data, therefore, help to define requirements for specific nucleotides in interior joining regions near the core.

Utilization of both phosphorylation sites in 58 nt ribozyme K28(1–77)C

At 58 nt in length, ribozyme K28(1–77)C is less than half the length of the original K28 ribozyme and was the shortest ribozyme tested (Figure 5A). This ribozyme was also among the most active, converting about two-thirds of the input RNA into thiophosphorylated product with an apparent first-order rate constant (k_{obs}) of $0.00322 \pm 0.00010\,min^{-1}$ (Figure 5B). To determine whether both phosphorylation sites are used, ribozyme K28(1–77)C was transcribed non-radioactively, then was allowed to self-phosphorylate in the presence of [γ-^{32}P]GTP, followed by digestion with DNAzyme Dzy5. As with the full-length ribozyme, this treatment yielded two radioactive fragments of sizes 40 and 18 nt indicating that truncating K28 from 126 nt to 58 nt in no way impeded the ribozyme's ability to use both sites. To determine the generality of dual-site utilization, 18 active variants of ribozyme K28 were transcribed non-radioactively and treated as mentioned earlier. All 18 mutants retained phosphorylation at both sites (Table 1, Supplementary Figure S4 and data not shown). Intriguingly, the relative utilization of the downstream target site increased roughly 2-fold for the shortened molecules. In particular, although K28(1–98) showed relative percentages of SP of approximately 77 and 23% for the 5′-most and 3′-most target sites, respectively (site preference ratio ~3), ribozymes K28(1–77)C and other RNAs of similar length showed a more even utilization of the two sites (site preference ratio ~1.4). Importantly, the retention of dual-site labeling in all active mutants support a functional relationship between the roles of the two sites in the overall mechanism of the ribozyme.

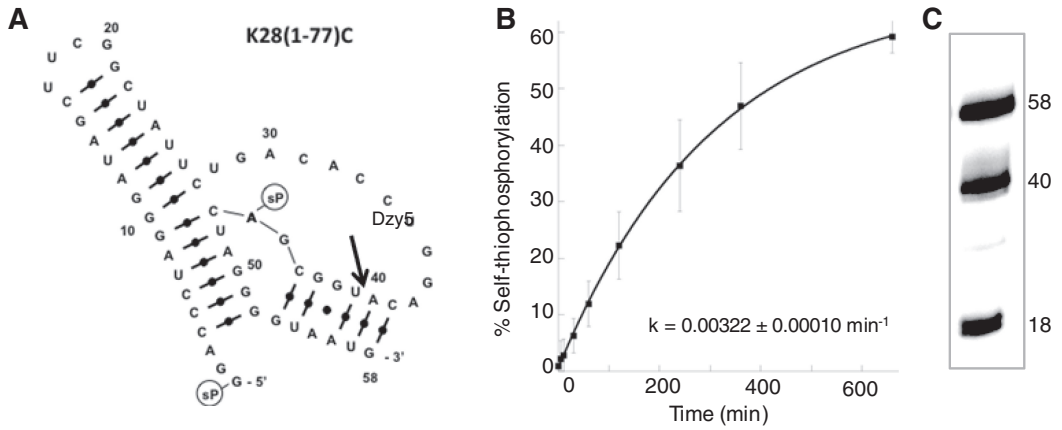

Figure 5. A 58-nt ribozyme with dual-site kinase activity. (**A**) Secondary structure of ribozyme K28(1–77)C. Arrow indicates the cleavage site of DNAzyme Dzy5. (**B**) Self-thiophosphorylation of ribozyme K28(1–77)C was monitored in the presence of 1 mM GTPγS in SP buffer. Plotted values are the average fraction converted to product at each time point from three independent kinetic experiments. Vertical error bars reflect standard deviations among these measurements. These averaged values were used to compute the apparent first-order kinetic rate constant (k_{obs}). Reported error in k_{obs} reflects the uncertainty of the fit. (**C**) Ribozyme K28(1–77)C was allowed to self-radiolabel, then digested with DNAzyme Dzy5, as detailed in figure 1 and in the text. Because of the internal deletion relative to ribozyme K28(1–77), the two labeled cleavage fragments are 40 and 18 nt in length for ribozyme K28(1–77)C. Accumulation of radiolabel in both cleavage fragments indicates that this small ribozyme retains phosphoryl transfer activity at both phosphorylation sites.

Comparison between products of self-labeling and products of PNK

The kinetic analyses mentioned earlier used trilayer gels in which the middle layer contained a high concentration of covalently embedded mercury (typically 100 μg/ml APM) to trap sulfur-containing product at the interface between the top and middle layers (27,28). In contrast, when gels contain very low levels of APM throughout the gel (e.g. 0.1 μg/ml APM), sulfur-containing RNA molecules continue to migrate through the gel with reduced electrophoretic mobility. The degree of retardation is a function of the number of sulfur atoms per strand and the influence of their chemical environments on the electron-donating potential of the sulfur atom, with mobility decreasing in the order thiols > internal non-bridging phosphorothioates >5′-gamma-thiotriphosphate (26). To gain more insight into the nature of the reaction catalyzed by ribozyme K28(1–77)C, we therefore compared the electrophoretic consequences of RNA-catalyzed thiophosphoryl transfer with those of 5′ thiophosphorylation by PNK.

Internally radiolabeled ribozyme K28(1–77)C was first dephosphorylated with CIP and then 5′-mono-phosphorylated with PNK in the presence of ATP (no sulfur) (Figure 6A). As expected, unreacted, CIP-treated and PNK-treated RNAs all co-migrated on a low-APM gel (Figure 6B, product 'f', compare Lanes 1, 2 and 3). A minor, unidentified product (band 'b') is also present. PNK treatment in the presence of ATPγS to generate 5′-mono-thiophosphorylated RNA produced a single major new band with reduced mobility (Figure 6B, Lane 4, product 'e'). RNA-catalyzed self-thiophorylation by overnight incubation of CIP-treated RNA with GTPγS yielded a different, single, major new band (product 'c') that migrated more slowly than the 5′ thiophosphorylated product of the PNK reaction (Figure 6B, compare Lanes 4 and 5). The reduced mobility of product 'c' indicates either that this RNA carries more than one sulfur within individual strands or that the chemical environments of thiophosphoryl groups acquired through self-labeling induces them to interact more strongly with the organomercurial matrix than does the 5′ thiophosphoryl species produced by PNK treatment alone. Partial degradation products 'g' and 'i' also accumulated on overnight incubation, due to the presence of divalent ions in the SP buffer.

In contrast, three new bands appeared when the PNK treatment of the self-thiophosphorylated product was carried out in the presence of ATPγS (Figure 6B, Lane 6, products 'a', 'd' and 'h'). The lower two of these likely reflect end labeling of degradation products 'g' and 'i', respectively, as they are shifted upwards by a similar degree to the shift observed in Lane 4. The diffuse band 'a' near the top of the lane barely migrated at all and appeared only in the sample that experienced both types of labeling (overnight self-labeling and PNK treatment). No change in the mobility pattern was evident when the same self-thiophosphorylated ribozyme was subsequently 5′ labeled by brief (30 min) PNK treatment with ATP (no sulfur; Figure 6B, Lane 7). If ribozyme K28 is

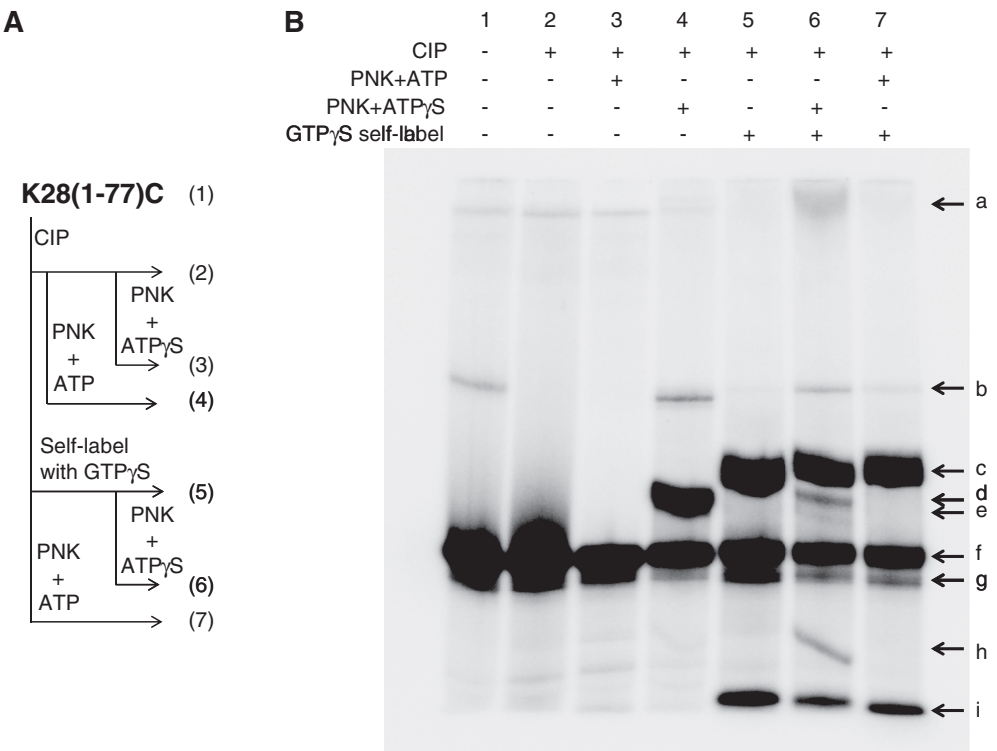

Figure 6. Probing the chemical environments of thiophosphorylated RNA. (**A**) Schematic of the enzymatic steps in sample preparation, as detailed in 'Materials and Methods' section. (**B**) Ribozyme K28(1–77)C was treated as indicated above the lanes. Lanes 1–7 correspond with 'samples 1 through 7', as detailed in 'Materials and Methods' section. Reaction products were analyzed on an 8% denaturing gel containing a low concentration of APM (0.1 mg/ml) throughout the gel. Arrows mark bands discussed in the text.

capable of acquiring two thiophosphoryl modifications within individual strands by self-kinase activity (Lane 5), then the very-low-mobility species in band 'a' may reflect the presence of three thiophosphoryl groups within individual strands of RNA. Electrostatic and steric clashes from the 2′ thiophosphate on G1 may reduce the suitability of this material as a substrate for subsequent labeling by PNK, thus resulting in the low-intensity signal from band 'a'. Furthermore, simultaneous 5′ and 2′ thiophosphorylation on the first nucleotide may favor formation of high-affinity chelation complexes with the immobilized mercury that greatly retard its mobility.

DISCUSSION

This work establishes that ribozyme K28 acquires a sulfur (in the presence of GTPγS) or a radiolabel (in the presence of [γ-^{32}P]GTP) at two different sites (Figure 1). In kinetic reactions using [γ-^{32}P]GTP as phosphoryl donor, radioactivity continues to be incorporated after overnight reaction (that is, new product is still being generated), whereas with GTPγS as donor, the reaction goes to completion in about half that time (E. Biondi *et al.*, submitted for publication). Thus, the reaction is substantially faster for GTPγS than for [γ-^{32}P]GTP, consistent with the transition state involving the gamma phosphate (mono-phosphoryl transfer) rather than the beta phosphate (pyrophosphoryl transfer), although the latter remains a formal possibility. Using a DNAzyme to cleave the RNA between the two phosphorylation sites after incubation with [γ-^{32}P]GTP allowed monitoring of radioactivity in both fragments (Table 1). Although full-length K28 favored utilization of the 5′ site (approximately 3:1 preference, see later), shorter variants used both sites more evenly (approximately 1.4:1 preference). The product of self-labeling with GTPγS migrates distinctly from the product of PNK labeling with ATPγS on gels with uniformly low concentrations of APM throughout the gel and combining both treatments yields a very low-mobility species (Figure 6B). These observations raise the intriguing possibility that individual RNA strands may acquire thiophosphoryl groups at both sites.

The site of thiophosphorylation near the 5′-end is assigned to nucleotide G1, as evidenced by radiolabeling of the shortest DNAzyme cleavage fragments (Figure 1B and C) and the continuous shifted alkaline digestion pattern down to nucleotide G2 on high-resolution sequencing gels (Figure 2A). The absence of a shifted band corresponding to G1 is consistent with blockage of phosphodiester exchange (strand cleavage) under alkaline conditions by thiophosphorylation of the 2′OH. The internal modification site is between nucleotides 60 and 74, based on the radiolabeling patterns retained after digestion with DNAzymes that cleave the RNA at various specific positions (Figure 1C and data not shown). There was no unambiguous gap in this region of the partial alkaline digestion pattern due to overlapping signal from individual molecules labeled on G1, precluding unambiguous assignment of the modification site. However, a thiophosphorylation-dependent RT pause at position U67 implicates nucleotide A65 or C66 (Figure 2B). Since the RT pause associated with G1 thiophosphorylation was located 2 nt before the modified nucleotide, we tentatively assign A65 as the internal site. Interestingly, a previous report noted RT pausing at the position immediately adjacent to a site of 2′OH thiophosphorylation (32). The earlier stop observed near G1 may be related to reduced affinity of the RT for primer/template substrates with very short 5′ single-strand overhangs. Although it is possible that a moiety other than the 2′OH acts as acceptor, such as a nucleobase N6 or N7, thiophosphorylation at these positions is expected to disrupt RT more severely than the pause that is observed here and to compromise amplification of such a ribozyme during *in vitro* selection. Thus, the 2′OH is also the most likely nucleophile on the internal acceptor nucleotide.

Enzymatic digestion (Figure 3) and mutational analysis (Figure 4) identified three helical elements that form a noncanonical H-type pseudoknot that includes a zero-length J1/3 connection. Truncations from the 3′-end established position 77 as the last nucleotide required for achieving maximal product yield; internal deletions generated ribozyme K28(1–77)C, which is the smallest active RNA identified here (58 nt, Figure 5). Interestingly, reducing the RNA size or increasing helical stability generally improved self-thiophosphorylation yield (Figure 4A). Most (9/12) of the single-stranded nucleotides near the structural core were perfectly conserved or very highly conserved on mutation and reselection, including nucleotide A65 at the putative internal phosphorylation site (Figure 4A and B and Supplementary Figure S3). As in the original selection (18), the reselection placed no demands on the number of sites that become thiophosphorylated. In principle, specialized subpopulations may be present among the reselected sequences that have lost the ability to phosphorylate at one or the other site; however, if this is the case, these most strongly conserved nucleotides must still be required for thiophosphorylation at both of the two target sites to have avoided mutational drift.

The observation that dual-site thiophosphorylation is retained in 18 of 18 variants of ribozyme K28—several of which include stems with compensatory mutations in both strands—makes it highly unlikely that the RNA adopts two separate global folds to phosphorylate the two sites. Instead, static geometry and dynamic motion of the ribozyme likely make major contributions to dual-site reactivity. Six base pairs separate the two phosphorylation sites. This is a little more than half a helical turn and potentially places both G1 and A65 on the same side of the helix, assuming a typical A-form helix in between. Furthermore, non-helical backbone geometries for the single-strand segments could easily bring the two 2′OH groups near to each other and near the gamma phosphate of the donor GTP (Supplementary Figure S5). Reactions at phosphate centers are highly sensitive to the oxygen–phosphorus distance (r) and the angle of attack (τ) between the acceptor-phosphorus and phosphorus-donor line segments (37). Thus, although proximity of the two acceptors may be a key factor enabling dual site reactivity, it is unlikely that one static

structure orients both acceptors for the same phosphoryl group. We speculate that this dilemma may be resolved through small-scale dynamic remodeling within the active site to align either G1 or A65 for efficient phosphoryl transfer at any given time.

Ribozyme K28 and its variants raise intriguing mechanistic and evolutionary questions. In a separate study (E. Biondi *et al*., submitted for publication), we recently found that K28(1–77)C exhibit a log-linear dependence on pH, unlike the previously characterized Kin.46 and 2PT3.2 ribozymes (15,16), and it is the first to require Cu^{2+} ions. Although it also exploits inner sphere contacts with Mg^{2+}, it is active in $[Co(NH_3)_6]^{3+}$, indicating that these ions play structural roles. From an evolutionary point of view, it is intriguing that complex reactivity such as thiophosphorylation of two different sites can arise within selections that placed no such demand on the evolving population. Most of the selected and natural ribozymes perform their respective chemistries on only one site. Two exceptions are the group I and group II self-splicing introns, both of which catalyze a 'first phosphodiester exchange' that separates the 5′ exon from the intron and then shift to a closely related conformation to carry out a 'second phosphodiester exchange' that joins the 5′ and 3′ exons and liberates the intron [reviewed in (38–43)]. However, those ribozymes are much larger and more complex than the relatively naïve kinase ribozymes described here. There is an adage among practitioners of *in vitro* selection, 'You get what you select for'. In the case of dual-site kinase ribozymes, we have gotten more than we selected for. The data presented here identify the nucleotides that become (thio)phosphorylated by dual-site kinase ribozyme K28, they define the sequence and secondary structural requirements for the reaction—including a greatly simplified variant, 58 nt K28(1–77)C—and they reveal details of the reaction itself (e.g., that both sites may acquire label within a given RNA strand). The next frontier will be to delineate the underlying mechanism by which a single ribozyme achieves dual-site labeling.

SUPPLEMENTARY DATA

Supplementary Data are available at NAR Online: Supplementary Table 1 and Supplementary Figures 1–5.

ACKNOWLEDGEMENTS

Mark Ditzler and Margaret Lange provided constructive feedback on the manuscript and insightful discussions during development of the project. David G. Nickens made the initial experimental observations suggesting dual site activity within ribozyme K28.

FUNDING

The National Aeronautics and Space Administration Exobiology Program [NAG5-12360 to D.H.B.]; National Science Foundation [CHE-1057506 to D.H.B.]. Funding for open access charge: NSF [CHE-1057506].

Conflict of interest statement. None declared.

REFERENCES

1. Tsukiji,S., Pattnaik,S. and Suga,H. (2003) An alcohol dehydrogenase ribozyme. *Nat. Struct. Biol.*, **10**, 713–717.
2. Tsukiji,S., Pattnaik,S. and Suga,H. (2004) Reduction of an aldehyde by a NADH/Zn^{2+} -dependent redox active ribozyme. *J. Am. Chem. Soc.*, **126**, 5044–5045.
3. Nissen,P., Hansen,J., Ban,N., Moore,P. and Steitz,T. (2000) The structural basis of ribosome activity in peptide bond synthesis. *Science*, **289**, 920–930.
4. Lohse,P.A. and Szostak,J.W. (1996) Ribozyme-catalyzed amino-acid transfer reactions. *Nature*, **381**, 442–444.
5. Illangasekare,M., Sanchez,G., Nickels,T. and Yarus,M. (1995) Aminoacyl-RNA synthesis catalyzed by an RNA. *Science*, **267**, 643–647.
6. Turk,R., Chumachenko,N. and Yarus,M. (2010) Multiple translational products from a five-nucleotide ribozyme. *Proc. Natl. Acad. Sci. USA*, **107**, 4585–4589.
7. Chumachenko,N., Novikov,Y. and Yarus,M. (2009) Rapid and simple ribozymic aminoacylation using three conserved nucleotides. *J. Am. Chem. Soc.*, **131**, 5257–5263.
8. Landweber,L.F. and Pokrovskaya,I.D. (1999) Emergence of a dual-catalytic RNA with metal-specific cleavage and ligase activities:The spandrels of RNA evolution. *Proc. Natl. Acad. Sci. USA*, **96**, 173–178.
9. Bartel,D.P. and Szostak,J.W. (1993) Isolation of new ribozymes from a large pool of random sequences. *Science*, **261**, 1411–1418.
10. Ekland,E.H. and Bartel,D.P. (1996) RNA-catalysed RNA polymerization using nucleoside triphosphates. *Nature*, **382**, 373–376.
11. Wochner,A., Attwater,J., Coulson,A. and Holliger,P. (2011) Ribozyme-catalyzed transcription of an active ribozyme. *Science*, **332**, 209–212.
12. Hati,S., Boles,A.R., Zaborske,J.M., Bergman,B., Posto,A.L. and Burke,D.H. (2003) $Nickel^{2+}$-mediated assembly of an RNA-amino acid complex. *Chem. Biol.*, **10**, 1129–1137.
13. Burke,D.H. (2004) Ribozyme-catalyzed genetics. In: Ribas de Pouplana,L. (ed.), *The Genetic Code and the Origin of Life*. Eurekah.com and Kluwer Academic/Plenum Publishers, Georgetown, TX, pp. 47–74.
14. Chen,X., Li,N. and Ellington,A. (2007) Ribozyme catalysis of metabolism in the RNA world. *Chem. Biodivers.*, **4**, 633–655.
15. Lorsch,J.R. and Szostak,J.W. (1995) Kinetic and thermodynamic characterization of the reaction catalyzed by a polynucleotide kinase ribozyme. *Biochemistry*, **34**, 15315–15327.
16. Saran,D., Nickens,D. and Burke,D. (2005) A trans acting ribozyme that phosphorylates exogenous RNA. *Biochemistry*, **44**, 15007–15016.
17. Saran,D., Held,D. and Burke,D. (2006) Multiple-turnover thio-ATP hydrolase and phospho-enzyme intermediate formation activities catalyzed by an RNA enzyme. *Nucleic Acids Res.*, **34**, 3201–3208.
18. Biondi,E., Nickens,D.G., Warren,S., Saran,D. and Burke,D.H. (2010) Convergent donor and acceptor substrate utilization among kinase ribozymes. *Nucleic. Acids Res*, **38**, 6785–6795.
19. Curtis,E. and Bartel,D. (2005) New catalytic structures from an existing ribozyme. *Nat. Struct. Mol. Biol.*, **12**, 994–1000.
20. Lorsch,J.R. and Szostak,J.W. (1994) *In vitro* evolution of new ribozymes with polynucleotide kinase activity. *Nature*, **371**, 31–36.
21. Li,Y. and Breaker,R.R. (1999) Phosphorylating DNA with DNA. *Proc. Natl Acad. Sci USA*, **96**, 2746–2751.
22. Wang,W., Billen,L.P. and Li,Y. (2002) Sequence diversity, metal specificity, and catalytic proficiency of metal-dependent phosphorylating DNA enzymes. *Chem. Biol.*, **9**, 507–517.
23. Schlosser,K., Lam,J. and Li,Y. (2009) A genotype-to-phenotype map of *in vitro* selected RNA-cleaving DNAzymes: implications for accessing the target phenotype. *Nucleic Acids Res.*, **37**, 3545–3557.
24. Burke,D. and Rhee,S. (2010) Assembly and activation of a kinase ribozyme. *RNA*, **16**, 2349–2359.

25. Cho,B. and Burke,D. (2006) Topological rearrangement yields structural stabilization and interhelical distance constraints in the Kin.46 self-phosphorylating ribozyme. *RNA*, **12**, 2118–2125.
26. Igloi,G. (1988) Interaction of tRNAs and of phosphorothioate-substituted nucleic acids with an organomercurial. Probing the chemical environment of thiolated residues by affinity electrophoresis. *Biochemistry*, **27**, 3842–3849.
27. Biondi,E. and Burke,D. (2012) Separating and analyzing sulfur-containing RNAs with organomercury gels. *Methods Mol. Biol.*, **883**, 111–120.
28. Rhee,S. and Burke,D. (2004) Tris(2-carboxyethyl)phosphine stabilization of RNA: comparison with dithiothreitol for use with nucleic acid and thiophosphoryl chemistry. *Anal. Biochem.*, **325**, 137–143.
29. Zuker,M. (2003) Mfold web server for nucleic acid folding and hybridization prediction. *Nucleic Acids Res.*, **31**, 3406–3415.
30. Parisien,M. and Major,F. (2008) The MC-Fold and MC-Sym pipeline infers RNA structure from sequence data. *Nature*, **452**, 51–55.
31. Santoro,S.W. and Joyce,G.F. (1997) A general purpose RNA-cleaving DNA enzyme. *Proc. Natl Acad. Sci. USA*, **94**, 4262–4266.
32. Lorsch,J.R., Bartel,D.P. and Szostak,J.W. (1995) Reverse transcriptase reads through a 2′-5′ linkage and a 2′-thiophosphate in a template. *Nucleic Acids Res.*, **23**, 2811–2814.
33. Patterson,J., Nickens,D. and Burke,D. (2006) HIV-1 reverse transcriptase pausing at bulky 2′ adducts is relieved by deletion of the RNase H domain. *RNA Biol.*, **3**, 163–169.
34. Knapp,G. (1987) Enzymatic approaches to probing of RNA secondary and tertiary structure. *Methods Enzymol.*, **180**, 192–212.
35. Krol,A. and Carbon,P. (1987) A guide for probing native small nuclear RNA and ribonuclear structures. *Methods Enzymol.*, **180**, 212–227.
36. Chang,T., Horng,J. and Huang,H. (2008) RNALogo: a new approach to display structural RNA alignment. *Nucleic Acids Res.*, **36**, W91–W96.
37. Soukup,G. and Breaker,R. (1999) Relationship between internucleotide linkage geometry and the stability of RNA. *RNA*, **5**, 1308–1325.
38. Pyle,A. (2010) The tertiary structure of group II introns: implications for biological function and evolution. *Crit. Rev. Biochem. Mol. Biol.*, **45**, 215–232.
39. Michel,F., Costa,M. and Westhof,E. (2009) The ribozyme core of group II introns: a structure in want of partners. *Trends Biochem. Sci.*, **34**, 189–199.
40. Dayie,K. and Padgett,R. (2008) A glimpse into the active site of a group II intron and maybe the spliceosome, too. *RNA*, **14**, 1697–1703.
41. Vicens,Q. and Cech,T. (2006) Atomic level architecture of group I introns revealed. *Trends Biochem. Sci.*, **31**, 41–51.
42. Woodson,S. (2005) Structure and assembly of group I introns. *Curr. Opin. Struct. Biol.*, **15**, 324–330.
43. Westhof,E. (2002) Group I introns and RNA folding. *Biochem. Soc. Trans.*, **30**, 1149–1152.